Subretinal Pigment Epithelial Deposition of Drusen Components Including Hydroxyapatite in a Primary Cell Culture Model

Matthew G. Pilgrim,[1,2] Imre Lengyel,[1,3] Antonio Lanzirotti,[4] Matt Newville,[4] Sarah Fearn,[5] Eszter Emri,[1,3] Jonathan C. Knowles,[2] Jeffrey D. Messinger,[6] Russell W. Read,[6] Clyde Guidry,[6] and Christine A. Curcio[6]

[1]UCL Institute of Ophthalmology, University College London, London, United Kingdom
[2]Division of Biomaterials and Tissue Engineering, UCL Eastman Dental Institute, University College London, London, United Kingdom
[3]Centre for Experimental Medicine, School of Medicine, Dentistry and Biomedical Science, Queen's University Belfast, Belfast, Northern Ireland, United Kingdom
[4]Center for Advanced Radiation Sources, The University of Chicago, Chicago, Illinois, United States
[5]Department of Materials, Imperial College London, London, United Kingdom
[6]Department of Ophthalmology, University of Alabama School of Medicine, Birmingham, Alabama, United States

Correspondence: Christine A. Curcio, Department of Ophthalmology, EyeSight Foundation of Alabama Vision Research Laboratories, 1670 University Boulevard, Room 360, University of Alabama School of Medicine, Birmingham, AL 35294-0019, USA; curcio@uab.edu.

CG and CAC are joint senior authors.

MCP and IL are joint first authors.

Submitted: November 4, 2016
Accepted: December 22, 2016

Citation: Pilgrim MG, Lengyel I, Lanzirotti A, et al. Subretinal pigment epithelial deposition of drusen components including hydroxyapatite in a primary cell culture model. *Invest Ophthalmol Vis Sci*. 2017;58:708–719. DOI:10.1167/iovs.16-21060

Purpose. Extracellular deposits containing hydroxyapatite, lipids, proteins, and trace metals that form between the basal lamina of the RPE and the inner collagenous layer of Bruch's membrane are hallmarks of early AMD. We examined whether cultured RPE cells could produce extracellular deposits containing all of these molecular components.

Methods. Retinal pigment epithelium cells isolated from freshly enucleated porcine eyes were cultured on Transwell membranes for up to 6 months. Deposit composition and structure were characterized using light, fluorescence, and electron microscopy; synchrotron x-ray diffraction and x-ray fluorescence; secondary ion mass spectroscopy; and immunohistochemistry.

Results. Apparently functional primary RPE cells, when cultured on 10-μm-thick inserts with 0.4-μm-diameter pores, can produce sub-RPE deposits that contain hydroxyapatite, lipids, proteins, and trace elements, without outer segment supplementation, by 12 weeks.

Conclusions. The data suggest that sub-RPE deposit formation is initiated, and probably regulated, by the RPE, as well as the loss of permeability of the Bruch's membrane and choriocapillaris complex associated with age and early AMD. This cell culture model of early AMD lesions provides a novel system for testing new therapeutic interventions against sub-RPE deposit formation, an event occurring well in advance of the onset of vision loss.

Keywords: hydroxyapatite, lipids, x-ray fluorescence, secondary ion mass spectrometry, x-ray diffraction

Age-related macular degeneration (AMD), the third largest cause of vision loss globally,[1] is expected to affect 288 million individuals worldwide by 2040.[2] The end stages of AMD are geographic atrophy and neovascular AMD. At present, there is no treatment for geographic atrophy.[3] End-stage neovascular AMD can be treated with regular injections of VEGF inhibitors,[4] a treatment that is costly to health care systems, burdensome for patients,[5] and possibly contributory to further atrophy.[4] Therefore, novel therapeutic intervention strategies should target early stages of AMD to prevent progression to advanced stages.

Early AMD is characterized by the presence of hallmark lesions that form between the basal lamina of the RPE and the inner collagenous layer of Bruch's membrane (BrM). These sub-RPE deposits can be focal (drusen) or diffuse (basal linear deposit [BLinD]) and are distinct from a diffuse thickening of the RPE basal lamina called basal laminar deposits (BLamD). Although drusen and BLinD are minimally present in normal aged human eyes, they are abundant in eyes with AMD. Drusen and BLinD confer risk for progression to neovascularization and RPE cell death.[6] Therefore, a strategy to prevent progression to late AMD is to modulate deposit formation and clearance. A better understanding of the molecular events leading to the retention of drusen components is essential for the success of this strategy. A model system that recapitulates as many aspects of drusen and BLinD formation as possible would accelerate progress toward these goals.

Sources of the molecular components of drusen and BLinD are not yet established, although candidates exist. An early hypothesis suggests that these lesions are formed from byproducts of photoreceptor outer segment phagocytosis by the RPE.[7] However, it was later postulated that a lipid-recycling pathway, driven by diet, of RPE-secreted lipoproteins is responsible.[8] Johnson et al.[9] showed that highly differentiated and well-polarized primary human foetal RPE cells (hfRPE) secreted several deposit-associated proteins without exposure to outer segments or choroidal blood flow. This supports the

idea that some components of deposits originate from the RPE and/or components derived from the culture medium. Proteomic analysis of isolated human drusen also implicated circulating plasma as a protein source.[10]

Regardless of source(s), it is important to understand what triggers the retention of lipids and proteins in the sub-RPE space. One potential mechanism is binding of RPE-produced lipids and lipoproteins to extracellular matrix elements including proteoglycans in BrM, a mechanism similar to plasma lipoproteins binding to arterial intima in atherosclerosis.[11] A second mechanism is retention of proteins via formation of large oligomers,[12] a process that is accelerated in the presence of trace metals like zinc.[13,14] A third mechanism is binding of proteins to the hydroxyapatite (HAP) spherules recently identified in the sub-RPE space and in drusen of humans.[15] Any of these or a combination may be operative.

Published cell culture models for sub-RPE deposit formation[9,16,17] each identified some, but not all, of the major molecular constituents of human sub-RPE deposits, lipids,[18,19] hydroxyapatite,[15] trace elements,[13,14] and proteins,[10,20] in a single model system. A molecularly and physically faithful model system should recapitulate these molecular constituents and form both diffuse and focal deposits. Here, we present evidence that primary RPE cells under standard culturing conditions can create such deposits. Thus, key physical and molecular signatures of AMD lesions, verified by histopathology and high-resolution molecular imaging, can be recreated in vitro by primary RPE cells in a standard medium and without supplementation by either retinal extracts or photoreceptor outer segments.

Materials and Methods

Primary RPE Cell Culture

Freshly enucleated porcine eyes were recovered from animals following unrelated physiology experiments, transported to the laboratory in ice-cold standard saline, and processed as described.[21] In brief, the eye was opened with a cut at the equator that avoided the vitreous body. With one pair of forceps, the anterior half of the eye, including the vitreous body, was lifted away from the posterior half of the eye. The posterior portion contained the retina, RPE/choroid, and sclera. The retina was gently removed with forceps. The RPE cells were released from the eyecups by treatment with trypsin 0.25% and EDTA 0.02% (Gibco, Grand Island, NY, USA). To avoid contamination with other cells, we performed a density gradient centrifugation through a cushion composed of Percol 40% (Pharmacia Biotech, Piscataway, NJ, USA) with 0.01 mol/L Na_2PO_4 and 0.15 mol/L NaCl, pH 7.4, at room temperature. After centrifugation, pigmented cells were recovered in the pellet, whereas unwanted cells remained near the top of the cushion. Primary RPE isolated from two porcine eyes were used to establish six Transwell cultures (24-mm polyester membrane, 0.4-μm pore size; Costar, Corning, NY, USA) without laminin or collagen coating. Cells were cultured in Miller medium[22] containing 1% fetal calf serum for up to 6 months, per the results. Medium was changed every 3 to 4 days. When applicable, primary cell cultures were subcultured every 2 weeks at a ratio of 1:2, meaning that one dish was divided into two identical dishes and then maintained under the same conditions.

Human Fetal RPE Cell Culture

Primary human fetal RPE cells (hfRPE; Sciencell, Carlsbad, CA, USA) were propagated in a T-75 flask (Corning; Thermo Fisher Scientific, Waltham, MA, USA) with Epithelial Cell Medium (EpiCM) (ScienCell), completed with 2% fetal bovine serum (ScienCell), 1:100 mL/mL epithelial cell growth supplement (ScienCell), and 107 U/L penicillin/10 g/L streptomycin (ScienCell). For our experiments, cells at passage 2 were cultured either on 10-μm-thick Transwell inserts with a pore diameter of 0.4 μm (Corning; Thermo Fisher Scientific) coated with Geltrex extracellular matrix (Thermo Fisher Scientific) or on 100-μm-thick Transwell inserts with a pore diameter of 0.45 μm (Millipore; Thermo Fisher Scientific) coated with laminin (Sigma-Aldrich Corp., St. Louis, MO, USA), in MEM-α modifications as previously described.[22]

Immunohistochemistry of Porcine Cells

Immunofluorescence was performed on flat mount and cross sections of porcine RPE cells using methods for cells on coverslips.[21] Cross sections shown in Figure 1 were 10 μm thick and were generated using a cryostat (Leica CM 3050 S; Leica, Bannockburn, IL, USA). Primary antibodies included cytokeratin 18,[23] zonula occludens,[24] apically localized Na^+-K^+ ATPase,[25] cellular retinaldehyde binding protein,[26] and microsomal triglyceride transfer protein.[27]

For apolipoprotein E (ApoE) staining, cultures were fixed in 4% paraformaldehyde with 1% glutaraldehyde, cryopreserved in 30% sucrose overnight, and then embedded in optimal cutting temperature compound (Agar Scientific, Stansted, Essex, UK). Cryosections, 10 μm thick, were generated using a cryostat (Leica CM 3050 S; Leica) and collected on glass slides. Cryosections were blocked with a 1:20 dilution of donkey serum in PBT (D9663; Sigma-Aldrich Corp.) for 1 hour at room temperature. Subsequently, sections were incubated with primary antibody followed by secondary antibody for 1 hour each. The primary antibody used was goat anti-ApoE polyclonal (1:500 dilution; #AB947; Millipore, Billerica, MA, USA) and the secondary antibody was an Alexa Fluor donkey anti-goat secondary antibody (1:200 dilution; excitation wavelength, 488 nm; A11055; Molecular Probes). To visualize nuclei, Hoechst nuclear stain (1:5000 dilution; excitation wavelength, 358 nm; H21492; Molecular Probes) was used. Samples were incubated for 20 minutes at room temperature and in the dark. Images were generated using a Zeiss LSM700 confocal microscope (Oberkochen, Baden-Württemberg, Germany) through a 63×/1.2 NA Zeiss Neofluar objective.

Immunohistochemistry of Human Fetal RPE Cells

Immunohistochemistry was performed according to the procedure described for porcine cells, except that human fetal RPE cells were cultured for 8 weeks and fixed in 4% paraformaldehyde before embedding and sectioning. Primary antibodies used in these experiments were against ApoE (1:200 dilution; AB947; Millipore) and/or ZO1 (1:400 dilution, 610966; BD Biosciences, Franklin Lakes, NJ, USA). Alexa Fluor 546-561 and 488 IgG (H+L) (1:200; 11056 and 21202; Molecular Probes) were used as secondary antibodies to detect anti-ApoE and anti-ZO1, respectively.

Synchrotron Microfocus X-ray Fluorescence and Microfocus X-ray Diffraction Analysis

Synchrotron microfocus x-ray diffraction (μXRD) and microfocus x-ray fluorescence (μXRF) analysis of cell cultures was collected at the 13-ID-E beamline at the Advanced Photon Source (APS), Argonne National Laboratory. Analytical methods and instrument configuration follow those described in Lanzirotti et al.[28] Porcine cell cultures were flat mounted on Kapton film for analysis. An incident beam energy of 17.48 keV

Investigative Ophthalmology & Visual Science

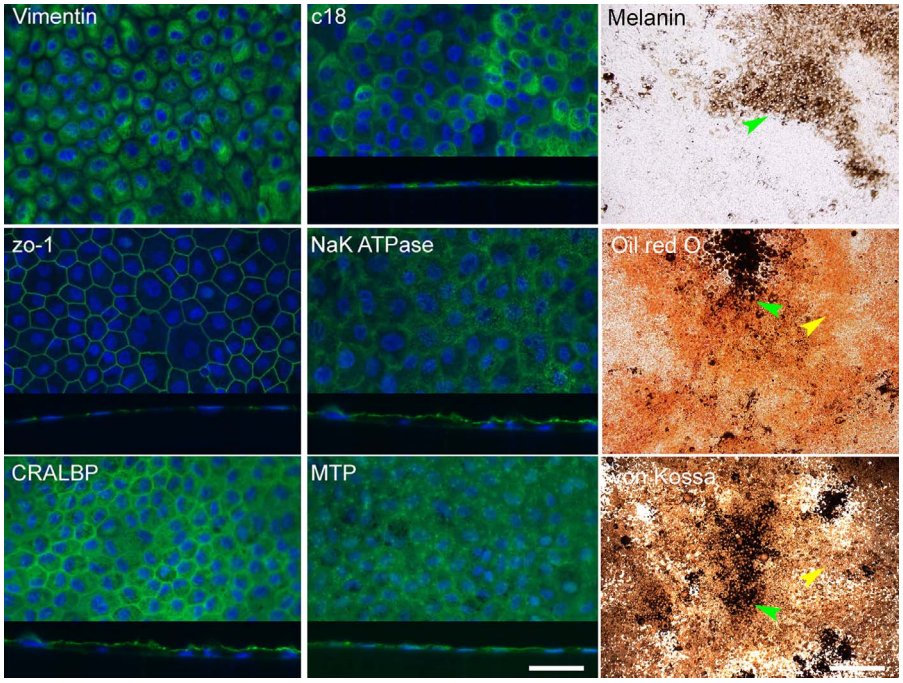

Figure 1. Primary porcine RPE cells are associated with lipids and phosphates 6 weeks after isolation. (**Left**, **middle**) Confluent monolayers exhibit polygonal cells with sharp vertices, orderly packing geometry, and strong localized immunofluorescence for known RPE-expressed proteins, viewed en face and in cryosections, including cytokeratin 18 (c18), Vimentin, zonula occludens (ZO-1), apically localized Na^{+}-K^{+} ATPase, cellular retinaldehyde binding protein (CRALBP), and microsomal triglyceride transfer protein (MTP; MIM 157147). (**Right**) (*Top*) Continuous lawn of melanized (*green arrowhead*) and nonmelanized RPE cells. (*Middle*) Oil red O stain show neutral lipids (*yellow arrowhead*). (*Bottom*) von Kossa method shows calcium phosphate (*yellow arrowhead*). *Scale bars* denote the following: *left* and *middle columns*, 50 μm; *right column*, 250 μm.

was used, focused to a spot size of $\sim 1 \times 2$ μm (H × V) with a photon flux of $\sim 10^{11}$ photons/s within this focused spot. X-ray fluorescence from the sample was measured using a four-element Vortex ME4 (Hitachi, Inc., Northridge, CA, USA) silicon drift diode detector coupled to an Xspress 3 digital x-ray multichannel analyzer system (Quantum Detectors, Harwell, Oxford, UK). X-ray diffraction from the sample was measured using a Perkin Elmer XRD1621 digital flat panel detector (Santa Clara, CA, USA) placed in transmission geometry.

Note, experiments should control for the artifactual appearance of μXRD signatures from the buffer systems used (Supplementary Fig. S1).

Identification of HAP, Protein, and Lipid by Time of Flight–Secondary Ion Mass Spectrometry Imaging

Secondary ion mass spectrometry (SIMS) and secondary ion mapping was performed using a TOF.SIMS5-Qtac^{100} LEIS mass spectrometer (ION-TOF, Münster, Germany). Submicrometer resolution was used for secondary ion mapping over m/z 0-880. The system is comprised of a bismuth primary ion beam, operating at 25 kV and tuned to use the Bi_3^+ cluster for greater secondary ion yield, and a low energy electron flood gun for charge compensation. Ionic species sputtered from the surface under the bismuth bombardment are steered into a reflectron time-of-flight mass analyzer. Before mass spectrometry was performed, an increased ion beam current was used to remove potential contamination from the upper surface of the sample. Identified peaks strongly localized to deposits were mapped on single ion maps.

Hydroxyapatite Fluorescent Labeling

Fixed and de-waxed paraffin embedded sections, 20 μm thick, with crystalline deposits were stained with 20 μM bone-tag 680RD (926-09374; Li-Cor) or 20 μM OsteoSense (NE-V10020EX; Perkin Elmer) in aqueous buffer for 20 minutes at room temperature. Samples were imaged using a Zeiss LSM700 confocal microscope through a 63×/1.2 NA Zeiss Neofluar objective with an excitation wavelength of 620 nm and emission wavelength of 680 nm.

Transmission Electron Microscopy

Culture dishes were preserved in cold 1% glutaraldehyde, 2.5% paraformaldehyde, in 0.1 M phosphate buffer and photo-documented using a dissection microscope with a dark-field illumination base. Transwell inserts with cells attached were cut into 2 × 2 squares, photodocumented for orientation, postfixed by the osmium tannic acid paraphenylenediamine method to accentuate neutral lipid,[19] sectioned at silver-gold thickness, and viewed with a 1200 EXII electron microscope (JEOL USA, Peabody, MA, USA) and an AMTXR-40 camera (Advanced Microscopy Techniques, Danvers, MA, USA).

Scanning Electron Microscopy

Fixed cell cultures stored in PBS were dehydrated in a graded ethanol series (20%, 50%, 70%, 90%, and 100%) before critical point drying in hexamethyldisilazane (Sigma-Aldrich Corp.). Samples were mounted using carbon adhesive tabs on aluminium stubs (Agar Scientific). Specimens were sputter coated with gold/palladium and imaged using a Philips XL30

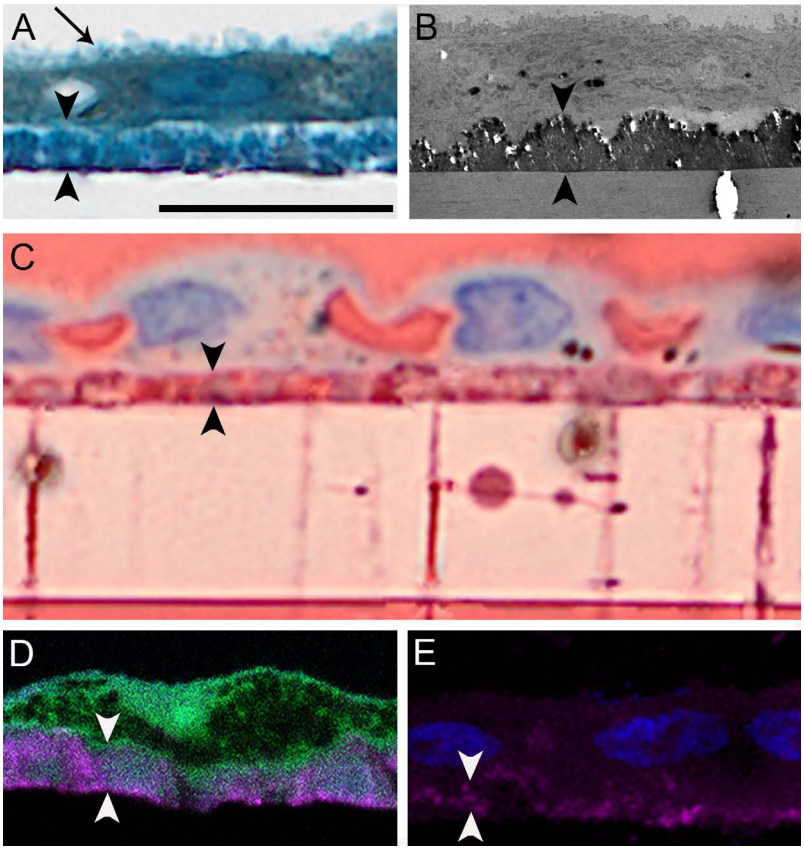

Figure 2. Lipids and calcium localize to sub-RPE deposits. (**A**) Primary porcine RPE cells cultured for 12.0 weeks are confluent. They exhibit a brush-border apically (*arrow*) and overlie a diffuse deposit (*arrowheads*). One-micrometer epoxy section, toluidine blue stain. (**B**) Deposit is a continuous and electron dense monolayer without evidence of thickened basal lamina; transmission electron microscopy. (**C**) Deposits contain neutral lipid, as do pores crossing the Transwell insert. Oil red O stain. (**D**) Cells form a continuous layer over HAP (*magenta*) positive deposits. Cryo-section; cells, autofluorescence; HAP deposit, bone-tag680RD (Li-Cor) fluorescent stain. (**E**) Deposits under nucleated cells (*blue*) contain HAP (*magenta*). Cryo-section, bone-tag680RD for HAP and 4′,6-diamidino-2-phenylindole (DAPI) for nucleic acids (*blue*). *Scale bar* denotes 20 μm and applies to all panels. Images in **A** and **C** were matched in magnification to images obtained with higher-resolution imaging technologies in **B**, **D**, and **E** and thus exhibit empty magnification.

FEG-SEM (Hillsboro, OR, USA) with a spot size of 3 and an accelerating voltage of 5 kV.

Microcomputed Tomography

Samples were dehydrated as described for scanning electron microscopy. Dehydrated samples were mounted on to a rotary stage using an adhesive. Microcomputed tomography (micro-CT) was performed within a Philips XL30 FEG-SEM using the SkyScan μCT system (Bruker System, Billerica, MA, USA). Samples were scanned every 1.0° through 180.0°. Resolution was 1 μm per pixel. Three-dimensional reconstruction of scanned slices was achieved by volume rendering using the CTVox reconstruction software (Bruker System).

Human Eye Pathology

The Institutional Review Board at the University of Alabama at Birmingham approved the use of human tissue. Short postmortem (<6 hour) donor eyes used in prior publications were reviewed to identify deposits containing lipids, refractile material, and von Kossa–positive material. These include 82 AMD maculas (53 late AMD and 29 early AMD) processed for high-resolution submicrometer sections for the Project MACULA website of AMD histopathology[29,30] (http://projectmacula.cis.uab.edu/); geographic atrophy eyes (n = 10) stained with the von Kossa method[31]; and early and advanced AMD eyes (n = 12) stained for lipids and with the von Kossa method.[32,33] Selected areas were imaged using 60× oil immersion objectives (numerical aperture, 1.40). Images were montaged, composited, and adjusted for exposure, contrast, and sharpness (Photoshop CS6; Adobe, San Jose, CA, USA).

Study Approval

Use of porcine eyes was approved by the Institutional Animal Use and Care Committee at the University of Alabama at Birmingham.

Results

Primary Cell Cultures Display Characteristics of Well-Differentiated Cells

At 1 day after isolation, clumps of heavily pigmented cells were attached and well spread on porous polyester Transwell membranes (Costar). Seven days after isolation, rapidly proliferating cells formed larger clumps and maintained cell–cell contacts and epithelioid morphology. By 14 days and thereafter, still-polygonal cells formed a confluent monolayer with high (>150 MΩ) trans-epithelial resistance, a comprehensive measure of RPE polarity, confluence, and integrity of cell–cell contacts.[22] Whether examined en face or as vertical cryo-

Investigative Ophthalmology & Visual Science

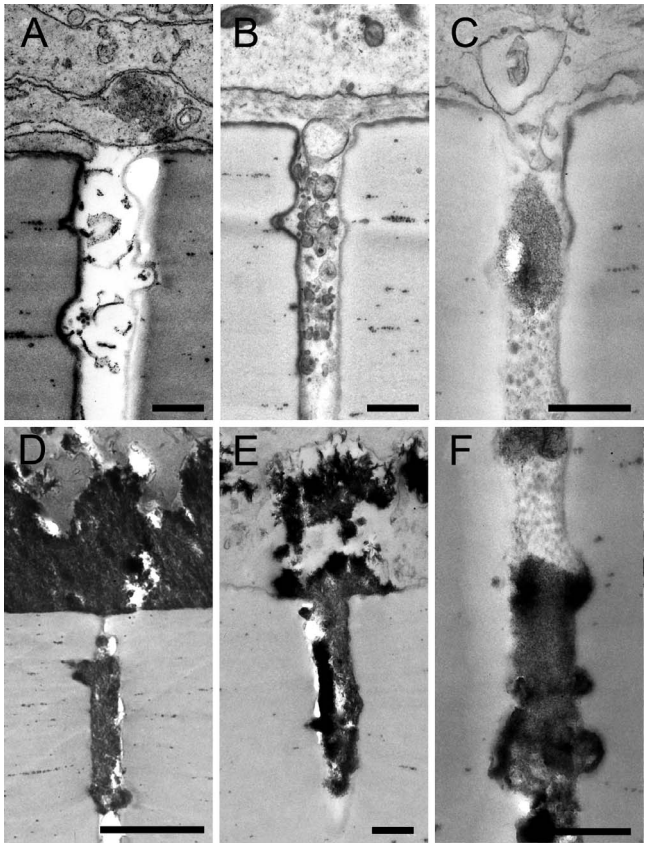

FIGURE 3. Retinal pigment epithelium–secreted materials in Transwell insert pores (0.4 μm diameter). Electron microscopy revealed cellular processes and material of varying electron density within the pores of the cell culture insert. (**A**) Membranous material in a pore under deposit-incapable cells at 6.0 weeks, indicating that these cells release material in culture, although not in sufficient quantity to accumulate. Cells in panels **B** through **F** are deposit-capable. (**B**) Spherical particles (26.5 weeks) demonstrating continuity of sub-RPE deposit into pores. (**C**) Cellular processes can enter Transwell pores alongside heterogeneous material (26.5 weeks). (**D–F**) Accumulation of material with varying electron density accumulates in pores in apparent continuity with sub-RPE deposits.

sections (Fig. 1, left and middle columns), confluent monolayers showed strong immunoreactivity for markers of intermediate filaments, junctional complexes, polarized ion transporters, retinoid processing, and lipoprotein assembly, which are features that typify RPE in situ.

These primary cultures were associated with intermittent patches of lipid and phosphate deposition revealed by classic histochemical stains (Fig. 1, right column). Cells at 6.0 weeks were hexagonal especially in areas with high melanosome content (Fig. 1, Melanin). At this time, staining with oil red O was prominent near the pigmented cells (Fig. 1, Oil red O). von Kossa staining produced a patchy light brown reaction product suggesting mineralization was also present (Fig. 1, von Kossa).

Examination of Sub-RPE Deposits With Light, Fluorescent, and Electron Microscopy

Cells were well differentiated, as evidenced by numerous apical processes (Figs. 2A, arrow, 2B). A layer of toluidine blue–stained material between the RPE cells and the cell culture insert was observed (Fig. 2A). This material was electron dense (Fig. 2B) and unaccompanied by thickening of the basal lamina. Additionally, intense oil red O staining confirmed the presence of neutral lipids within the deposits and within the pores of the culture dish insert (Fig. 2C). Staining of pores was not detectable in inserts of dishes lacking cells. Electron microscopy also revealed the presence of cellular processes and material of varying electron density within pores (Fig. 3). Fluorescent dye staining for HAP indicated varying degrees of mineralization below the RPE (Figs. 2D, 2E). In all samples, deposits were confined to the sub-RPE compartment without equivalent deposits on the apical surface. Deposits were continuous on the spatial scale of several hundred cells but not across the entire dish and, as such, are referred to as diffuse.

Analysis of Sub-RPE Deposits With Electron Microscopy and Micro-CT

Next, we examined deposits at higher resolution using transmission electron microscopy (Figs. 4A–D) and scanning electron microscopy (Figs. 4E–H). Additionally, micro-CT was used for detection of mineralization (Figs. 4I–L). By following cultures over time, showed it was determined that passaged cells did not develop deposits under these experimental conditions, and thus these cells are designated deposit-incapable. Cell cultures were examined at three time points in culture and in two differentiation states: 6.0 weeks (deposit-incapable third passage cells), 6.0 weeks (deposit-capable primary cells), 12.0 weeks (primary cells with deposits), and 26.5 weeks (primary cells with abundant focal and diffuse deposits). Deposit-incapable passaged cells cultured for 6.0 weeks lacked apical processes, tight junctions, melanosomes, deposits, and signal for mineralization (Figs. 4A, 4E, 4I). Deposit-capable primary cells at 6.0 weeks exhibited sparse, short, and stubby apical processes and formed apically located

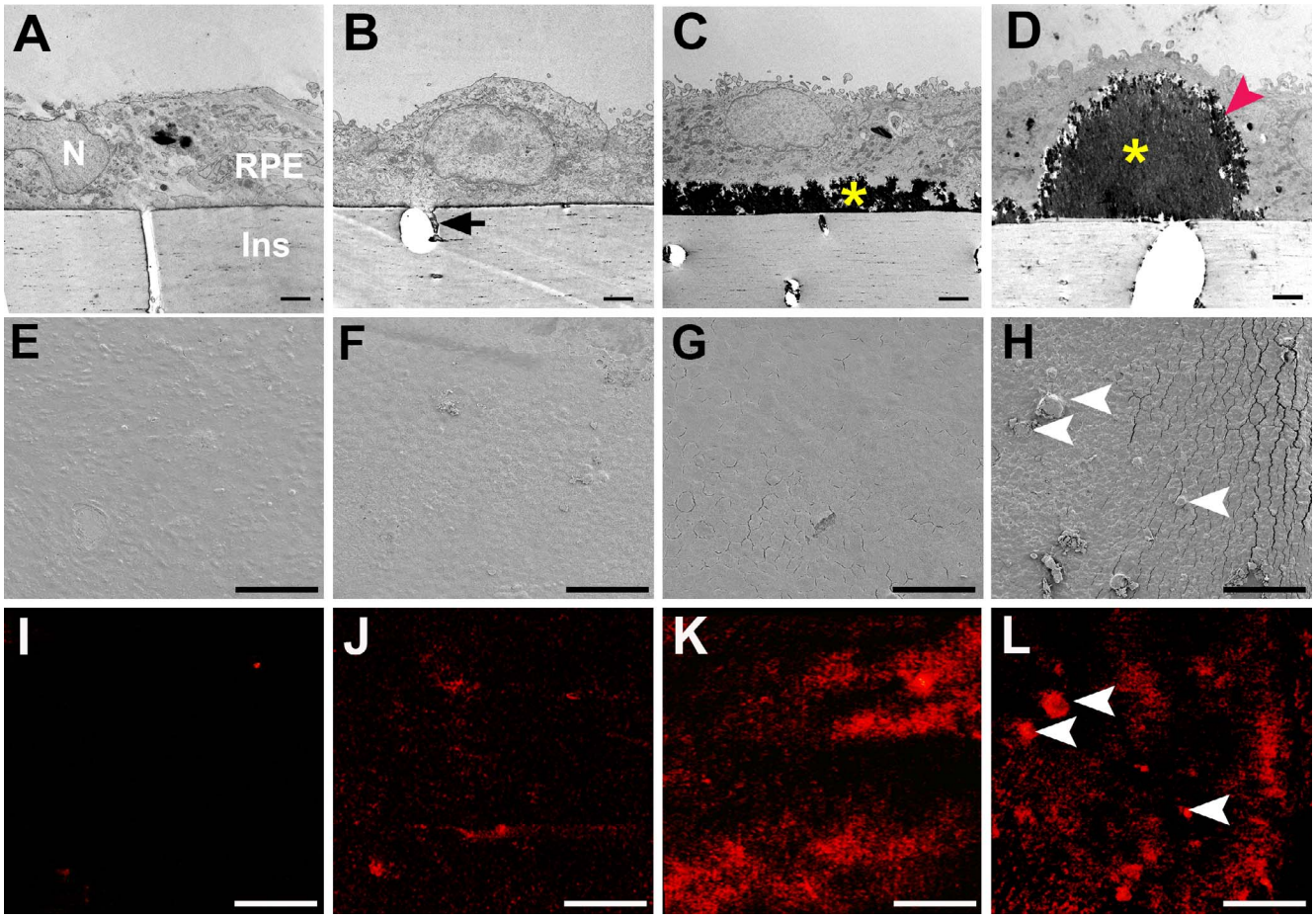

FIGURE 4. Evolution of mineralized deposits under porcine RPE in culture. Transmission electron microscopy (**A–D**), scanning electron microscopy (**E–H**), and microcomputed tomography for minerals (**I–L**). (**A**, **E**, **I**) Deposit-incapable, passaged cells at 6 weeks exhibited little or no mineralization. N, nucleus; Ins, culture dish insert. (**B**, **F**, **J**) Deposit-capable primary cells at 6 weeks produced a thin electron-dense sub-RPE deposit that was continuous with material in pores (*arrow*) and exhibited some mineralization. Due to the sectioning plane, the pore does not cross the Transwell. (**C**, **G**, **K**) At 12 weeks, deposit-capable cells developed a continuous layer of deposit with increased mineralization. (**D**, **H**, **L**) At 26.5 weeks, focal dome-shaped deposits were also present, with diffuse deposit, exhibited intense mineralization (**H**, **L**; *arrowheads*). Diffuse and focal deposits had solid cores (*yellow asterisks*) with feathery surfaces (*red arrowhead*) (**C**, **D**). Cracks between cells (**G**, **H**) are due to brittleness conferred by mineralization. *Scale bars* denote the following: **A–D**, 2 μm; **E–L**, 100 μm.

tight junctions and variable melanosome content. The cells also formed deposits that were not readily visible by transmission electron microscopy (Fig. 4B) but were clearly detected by micro-CT (Fig. 4J). Deposit-capable primary cells at 12.0 weeks exhibited numerous apical processes, many melanosomes, and extensive 2- to 3-μm-thick diffuse deposits (Fig. 4C) with strong and extensive mineralization (Fig. 4K). Deposit-capable primary cells at 26.5 weeks exhibited branching apical processes, extensive melanization, diffuse deposition, and numerous large, thick, dome-shaped deposits (Fig. 4D, red arrowhead). These deposits were focal, identifiable on scanning electron microscopy (Fig. 4H, arrowheads), intensely mineralized (Fig. 4L, arrowheads), and occasionally seen at 12 weeks. Diffuse and focal deposits were electron dense with solid interiors and feathery surfaces (Figs. 4C, 4D) and were highly refractile (Fig. 5).

Elemental and Mineral Characterization of Deposits Using μXRF and μXRD

We analyzed the elemental composition of cell culture deposits using μXRF (Fig. 6). The deposits produced by the cultured RPE cells were enriched in Ca (Figs. 6B, 6C), Fe (Fig. 6D), and Zn (Fig. 6E). Furthermore, the mineral content of deposits was determined through implementation of μXRD. The summed μXRD patterns (Fig. 6H) and corresponding radial intensity profiles (Fig. 6G, blue line) clearly identified the presence of HAP compared with a reference HAP 2θ profile (Fig. 6G, red bars). Mapping mode μXRD of the integrated intensity peaks representing the HAP 002 and 211 crystallographic reflections (Figs. 6I, 6J) showed that HAP was present throughout all examined focal deposits. Mapped HAP reflections were also observed between focal deposits, suggesting the presence of diffuse deposits within the examined area. These data provide evidence that primary RPE cells are capable of developing HAP-containing sub-RPE deposits that also contain Fe and Zn.

Characterization of Deposits Using SIMS

To determine whether deposits in culture also contain other constituents of human sub-RPE deposits, we analyzed sections of cultured cells containing visible focal deposits using SIMS. Typical ionic signatures for HAP (Supplementary Fig. S2A) and proteins (Supplementary Figs. S2B–S2E; represented by amino acids) were readily identifiable within nodules. Secondary ion

Investigative Ophthalmology & Visual Science

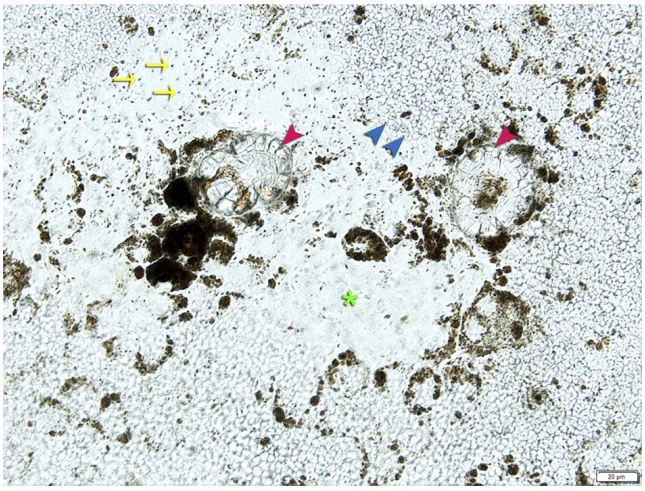

Figure 5. Diffuse and focal refractile deposits in a Transwell culture dish. Primary porcine RPE cells cultured ≥12 weeks overlie refractile focal (*red arrowheads*) and diffuse (*blue arrowheads*) deposits. The majority of cells are not strongly pigmented. Some cells lack melanosomes completely (*green asterisk*) as is common in RPE cell cultures. Pores through the Transwell insert are visible in places where cells are not present (*yellow arrows*).

mapping of HAP (Figs. 7B, 7C, represented by Ca^{+} and $Ca_2PO_4^{+}$, respectively), protein (Figs. 7E–H; demonstrated by glycine, alanine, proline, and leucine, respectively), and lipid (Fig. 7D; represented by phosphatidylcholine) confirmed the presence of these major molecular components of human sub-RPE deposits in deposits produced by our cell culture model.

Immunohistochemistry Confirms the Presence of Drusen-Related Proteins in Cell Culture Deposits

To confirm the presence of proteins within deposits and to corroborate that the presented cell culture system models early AMD, an immunohistochemical study was conducted using a polyclonal antibody against ApoE, a known marker of drusen and BLinD, and confocal microscopy. Punctate labeling of ApoE immunoreactivity was observed within focal deposits produced by cells cultured for 26.5 weeks (Fig. 8A, arrowheads). Furthermore, ApoE-immunoreactive diffuse deposition on the surface of the Transwell insert was also observed (Figs. 8A, 8B, arrows). Cells cultured for 26.5 weeks labeled with ApoE were also stained by a HAP-specific dye (OsteoSense; Perkin Elmer). Colabeling showed punctate ApoE deposition (Fig. 8C, green, arrows) within and below HAP deposits (Fig. 8C, magenta). Thus, deposits produced by apparently functional primary cell cultures have molecular characteristics similar to that of in vivo sub-RPE deposits.

This investigation used a polyester Transwell insert similar to that of Fernandez-Godino et al.[17] that is physically distinct from inserts used by Johnson et al.[9] We investigated whether the insert used in our model system contributed to the difference in deposition observed between our cell cultures and the punctate deposition seen by Johnson et al.[9] Human fetal RPE cells were grown on 10-μm-thick polyester Transwell inserts (Fig. 8D) and on 100-μm-thick porous membranes (Fig. 8E). Deposition of ApoE can be observed on the surface of the polyester Transwell insert (Fig. 8D, green). In contrast, when cells were cultured on 100-μm-thick porous inserts, only punctate deposition of ApoE within membrane cavities was observed (Fig. 8E, green), and a layer of diffuse deposits was absent.

Discussion

Herein, we demonstrated that well-differentiated primary porcine RPE cells in culture produce focal and diffuse sub-RPE deposits that contain HAP, lipids, proteins, and trace metals, as in deposits in human AMD macula. Deposits have been an elusive aspect of AMD pathology in model systems to date. To our knowledge, this is the first time that these four major molecular constituents have been replicated and confirmed in a single cell culture system, albeit with physical forms resembling, but not yet identical to, sub-RPE deposits in vivo. These achievements are significant for the molecular basis of AMD's specific lesions, RPE cell biology, and the prospects of a high-fidelity model system suitable for basic and translational AMD research.

Our experiments used 10-μm-thick polyester membrane inserts that imposed a physical barrier against movement of RPE secreted material or material present in the basal compartment of the culture medium. Our observations can be compared and contrasted with those of Fernandez-Godino et al.,[17] who reported that primary mouse RPE cells after 2 weeks in culture released material into 0.4-μm-diameter pores connecting apical and basal chambers, with cellular processes ramifying on the opposite side of the insert. Although we occasionally observed cellular processes in pores (Fig. 3), we observed extracellular deposits primarily between the RPE cells and the insert. Amin et al.[16] showed extracellular material between ARPE-19 cells and a smooth surface without pores or a basal compartment after 11 weeks. Using fetal human RPE cells on 100-μm-thick porous supports (PIHA 01250; Millipore), Johnson et al.[9] demonstrated particulate deposition of ApoE-immunoreactive secreted material exclusively within the insert and not on the insert surface. We also achieved particulate ApoE-immunoreactive deposition by human fetal RPE when using an identical insert. Importantly, when using a 10-μm-thick polyester membrane, we showed that these same cells produced extensive deposits on the insert surface (Fig. 8D).

Differences among cell culture systems are important to consider when extrapolating to the in vivo situation. Our data highlight the role of physical entrapment of material by aged BrM.[34] In the eye, the "insert" to which the RPE basal lamina attaches is the inner collagenous layer of BrM. In aging macula, inner and outer collagenous layers of BrM thicken[35,36] and accumulate lipoprotein particles.[37] Additionally, via processes that may involve the *ABCC6* gene,[38] BrM elastic lamina calcifies.[7] Once lipids and calcium are deposited, BrM could act as a physical barrier that retains proteins and lipids between the RPE basal lamina and inner collagenous layer. In this environment, entrapped lipids, calcium, and phosphate could promote HAP spherule formation,[15] to which monomeric and/or oligomerized proteins could bind.[12] It will be interesting to determine whether manipulation of the insert surface will promote deposit formation. Although our data indicates that a barrier is essential for formation of deposits, our studies do not address the relative contributions of aging BrM and choriocapillaris[39–41] to this barrier. Cocultures of RPE and choriocapillary endothelium may thus prove informative.

It is interesting to compare the deposits within our cell culture system to human AMD extracellular lesions (Fig. 9; Supplementary Table 1). Deposits in culture appear to model BLinD (lipid-rich linear deposits that can contain refractile nodules; Fig. 9A, arrowhead), basal mounds (BLinD material within BLamD; Fig. 9B), and early-stage hard drusen (lipid-rich and von Kossa–positive deposits; Figs. 9C, 9D). The solid appearance of deposits in culture suggests the lipid content is formed of lipoproteins.[8,42] rather than the accumulation of membranous material that was previously postulated.[43,44] As discussed,[8] membranes alone cannot account for oil red O

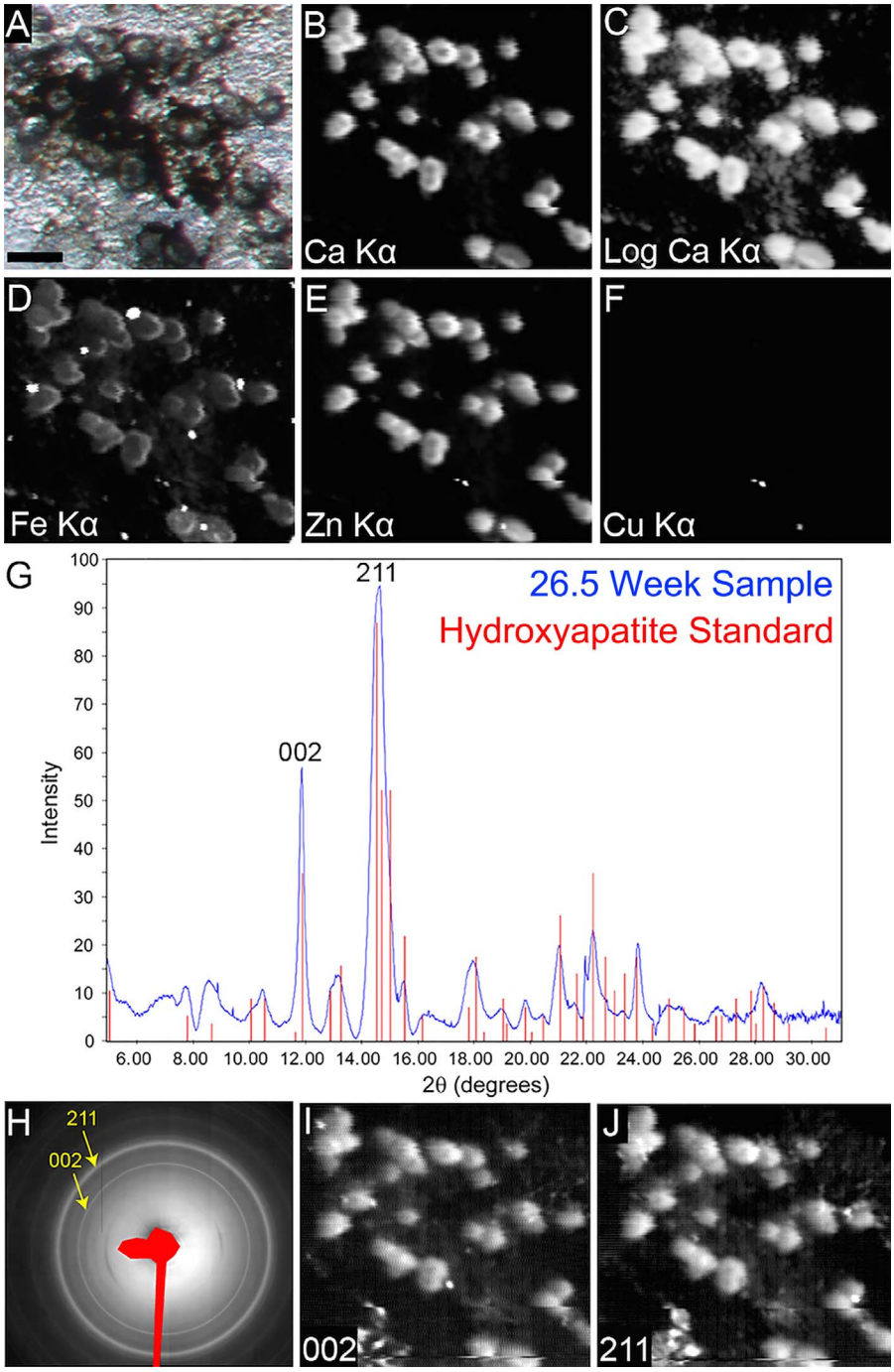

Figure 6. Analysis of diffuse and focal sub-RPE deposits by μXRF and μXRD. Reflected light photomicrograph of the area (**A**) where μXRF (**B–F**) and μXRD (**G–J**) patterns were obtained. Focal deposits contain calcium (Ca) (**B**), iron (Fe) (**D**), and zinc (Zn) (**E**). Copper (Cu) content was not well resolved in these measurements (**F**), suggesting that as in human cadaveric deposits, the Cu content is low or absent.[14] A logarithmic transformation of Ca Kα μXRF shows low-intensity signal diffusely distributed among the focal deposits (**C**). Summed μXRD (**H**) and the radial intensity profile (**G**; *blue line*) confirm the presence of HAP in sub-RPE deposits. *Red bars* in **G** represent reference HAP μXRD reflections (joint committee on powder diffraction standards [JCPDS] card 00-009-0432). Plotting the HAP characteristic diffraction peaks (002) and (211) confirmed the presence of HAP in focal and diffuse deposits (**H–J**). *Scale bar* denotes the following in A: 50 μm, which applies to **A–F**, **I**, and **J**.

binding lipid (including esterified cholesterol) in soft drusen. In contrast, deposits reminiscent of subretinal drusenoid deposits (between apical RPE and photoreceptors[45] lacking oil red binding lipid[33,46] and refractile bodies; Fig. 9A), BLamD (Fig. 9B), and end-stage drusen (aggregated refractile, von Kossa–positive nodules without histochemically detectable lipid; Figs. 9E, 9F) were absent from our culture system. These differences (Supplementary Table S1) underscore that further optimization is required to recapitulate all aspects of in vivo deposit formation. Fortunately, factors such as extracellular pH, concentration of extracellular calcium, phosphate, and trace metals,[47] lipid,[48] and protein[49] environments, and external factors such as supplementation can be easily tested and optimized in a cell culture system.

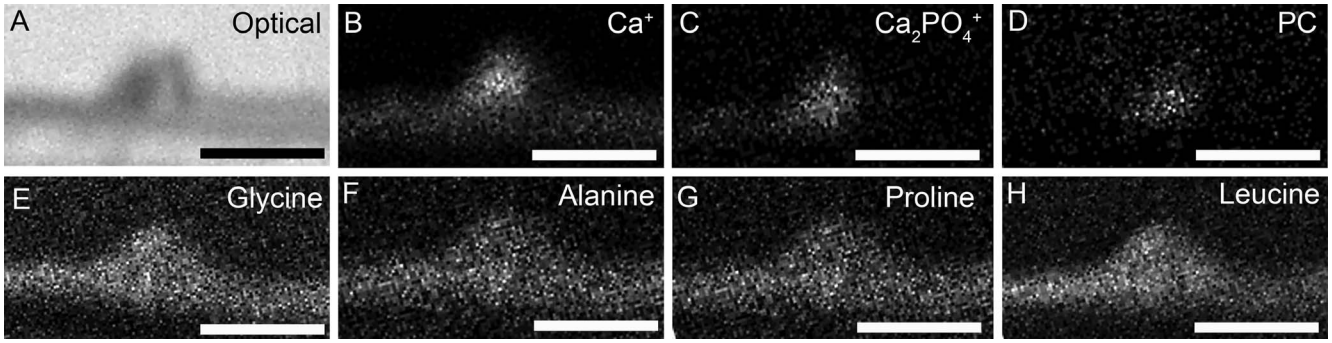

Figure 7. Distribution of the molecular ions identified by SIMS. An optical image of the focal deposit analyzed by SIMS analysis (**A**). Molecular ion mapping of calcium (Ca^+) (**B**) and calcium phosphate ($Ca_2PO_4^+$) (**C**) confirmed the presence of HAP within sub-RPE deposits. Lipid content of deposits was confirmed by molecular ion mapping of the phosphatidylcholine (PC) head group fragment ion (**D**). Mapping of amino acid signatures including glycine (**E**), alanine (**F**), proline (**G**), and leucine (**H**) confirmed the presence of protein within deposits. Thus, HAP, amino acids, and PC are all present within deposits. It should be noted that the culture insert is absent in the figure, during processing the cells and the sub-RPE deposits detached from the Transwell insert surface. *Scale bars* denote 40 μm.

There are two theories of drusen biogenesis[50]: transformation (direct conversion of RPE cells to druse material) and deposition (material released by an otherwise intact RPE cell layer). Our data support the latter theory, with the addition that material of RPE origin accumulates due to an outflow barrier in subjacent BrM.[34,51] The initial motivation for these experiments was the hypothesis that RPE secretes ApoB and E-containing lipoprotein particles in a constitutive and physiologic recycling system to dispose of excess lipids delivered by diet.[37,52] Cell autonomous secretion of lipid in our system, along with previously reported secretion of ApoE-immunoreactive lipoprotein-like particles[9] without outer segment supplementation, supports an overall physiologic and diet-driven model. This model is also supported by recent clinical imaging studies showing survival of the RPE layer over soft drusen for multiple years. Over this period, drusen increase in volume[53,54] and then collapse after the RPE layer disintegrates.[54]

In the porcine RPE system, early passage inhibited the ability of cells to form deposits, likely due to irreversible loss of phenotype via transdifferentiation.[21,55] This finding has implications not only for RPE model systems such as immortalized cell lines like ARPE-19, but also for replacement cells being considered for therapeutic transplantation.[56] Replacement cells might create deposits in the eye with deleterious consequences like those of native deposits. Conversely, transplanted cells that cannot produce deposits on an appropriate substrate may lack key cellular functions.

We demonstrated continuous sub-RPE deposits in the absence of many factors thought to be important in druse initiation. These include photoreceptor outer segments, human-specific serum components, non-RPE cells such as macrophages, RPE lipofuscin, BLamD, stress beyond that associated with isolation, exogenously applied injury, aging, and light exposure. Other factors not required are the gene for cholesterol ester transfer protein, an AMD risk factor [57,58] that

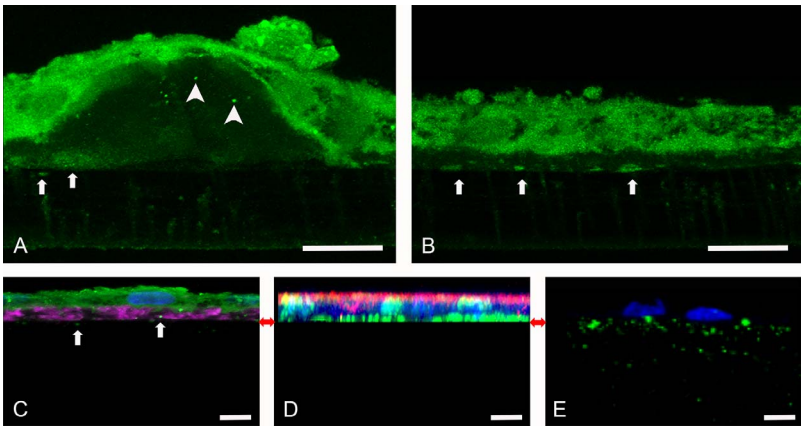

Figure 8. Accumulation of ApoE in sub-RPE deposits in primary porcine and human fetal RPE cell culture models. Immunohistochemistry was performed on porcine RPE cells cultured for 26.5 weeks (**A–C**) or on human fetal RPE cells cultured for 6 weeks (**D**, **E**). Transwell membranes were either polyester (**A–D**) or composed of mixed cellulose (**E**). (**A**) Punctate (*arrowheads*) and diffuse ApoE immunofluorescence was present within focal deposits, as well as on the surface of the polyester insert when cells were cultured for 26.5 weeks (*arrows*). (**B**) Apolipoprotein E–immunofluorescent deposits accumulated along the membrane in a nonuniform manner (*arrows*). Note the intense labelling within the RPE cells bodies and less intense labeling within pores of the Transwell membranes on **A** and **B**. (**C**) Punctate ApoE labeling (*arrows*) is found within or under HAP sub-RPE deposits (*magenta*). (**D**) Human fetal primary RPE cells grown for 8 weeks on polyester membrane inserts show ApoE (*green*) accumulation on the surface of the membrane, similar to that for porcine cells. Unlike porcine cells, human RPE cell bodies stain lightly for ApoE. Red immunofluorescence corresponds to ZO1 staining associated with junctions, indicating that the cells are well differentiated. (**E**) Human cells grown on membranes of mixed cellulose esters showed the dispersed accumulation of ApoE (*green*) particles, identical to those published by Johnson et al.,[9] in the membrane cavities. *Red arrows* between **C** and **E** indicate the surface of the membrane inserts. *Scale bars* denote 10 μm in **A–E**.

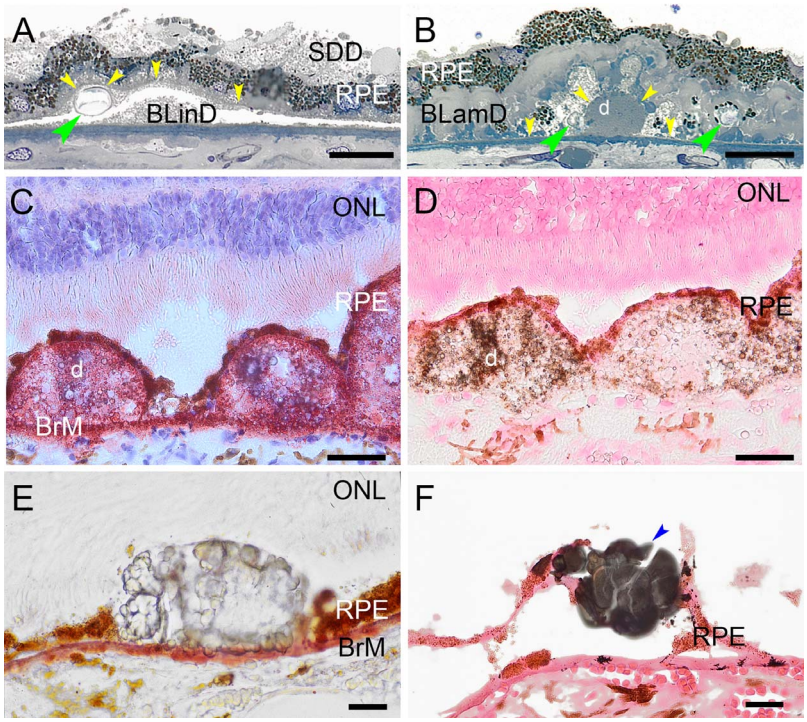

Figure 9. Lipids and calcium in human eyes with AMD. d, drusen. (**A**) Refractile nodule (*green*) localizes to BLinD (artifactually separated) and not to subretinal drusenoid deposit (SDD). *Yellow*, outer limit of BLamD. The osmium tannic acid paraphenylenediamine postfixation method stains extracellular lipid in BLinD gray, tan, or brown. (**B**) Refractile nodules (*green*) localize to basal mounds (soft druse material) within BLamD. (**C**) Hard drusen stained with oil red O has many spherules that are basophilic from hematoxylin staining. (**D**) Hard drusen with many von Kossa–positive spherules. (**E**) BrM is positive for esterified cholesterol and other oil red O–binding lipid. End-stage druse contains refractile nodules lacking detectable lipid. Overlying RPE and photoreceptors have atrophied. (**F**) Refractile nodules are von Kossa positive for calcium phosphates (*blue arrowhead*). *Scale bars* denote 50 μm in **A–D** and 20 μm in **E** and **F**.

is absent in pigs,[59] or any specific genotype. Without excluding direct deposition of culture medium components into the sub-RPE space, we can hypothesize that the minimum requirements for deposits are functional RPE cells that can secrete lipoproteins and molecules required for HAP formation, plus a retentive barrier.

The multiple molecular commonalities between in vitro deposits and human drusen provide impressive biological plausibility of this cell culture system. Questions to be addressed in future studies are generalizability to RPE from other species, time course of deposition, impact of outer segment supplementation, and a comprehensive molecular comparison of in vitro deposits versus human AMD lesions. Such data would support use of this model system for testing the regulation and therapeutic abatement of sub-RPE deposits. This is important because deposits provide a proinflammatory proangiogenic nidus and cleavage plane for neovascularization.[60] Reduction of drusen volume[61] through targeted therapies[62] has the potential to mitigate the treatment burden of VEGF suppression for neovascular AMD. Our culture system may be useful in achieving this goal.

Acknowledgments

The authors thank Lajos Csincsik and Po-Jung Pao for advice and technical assistance. Collaboration on this project was facilitated by the Arnold and Mabel Beckman Initiative for Macular Research.

Supported by National Institutes of Health Grants EY06109, unrestricted funds to the Department of Ophthalmology from Research to Prevent Blindness, Inc., and EyeSight Foundation of Alabama (CAC), and International Retinal Research Foundation (RWR). This project has also received funding from the "Eye-Risk" a European Union's Horizon 2020 research and innovation program under Grant 634479 and from the Bill Brown Charitable Trust Senior Research Fellowship, Moorfields Eye Hospital Special Trustees, Mercer Fund from Fight for Sight and Bright Focus Foundation (IL). The TOF-SIMS analysis was funded by the Engineering and Physical Sciences Research Council, UK (Grant EP/H006060/1) and by the Natural Environment Research Council, UK (Grant NE/J013382/1). Portions of this work were performed at the Advanced Photon Source (APS), Argonne National Laboratory at the GeoSoilEnviroCARS sector. GeoSoilEnviroCARS is supported by the National Science Foundation, Earth Sciences (EAR-1128799) and Department of Energy, GeoSciences (DE-FG02-94ER14466). Use of the Advanced Photon Source was supported by the US Department of Energy, Office of Science, Office of Basic Energy Sciences, under Contract DE-AC02-06CH11357.

CAC guarantees the integrity of the experiments, results, and analysis in this study and had full access to all of the data generated.

CAC and CG hold intellectual property related to this manuscript. The remaining authors declare that no conflict of interest exists.

Disclosure: **M.G. Pilgrim**, None; **I. Lengyel**, None; **A. Lanzirotti**, None; **M. Newville**, None; **S. Fearn**, None; **E. Emri**, None; **J.C. Knowles**, None; **J.D. Messinger**, None; **R.W. Read**, None; **C. Guidry**, P; **C.A. Curcio**, P

References

1. Resnikoff S, Pascolini D, Etya'ale D, et al. Global data on visual impairment in the year 2002. *Bull World Health Organ*. 2004; 82:844–851.
2. Wong WL, Su X, Li X, et al. Global prevalence of age-related macular degeneration and disease burden projection for 2020

and 2040: a systematic review and meta-analysis. *Lancet Global Health*. 2014;2:e106–e116.
3. Meleth AD, Wong WT, Chew EY. Treatment for atrophic macular degeneration. *Curr Opin Ophthalmol*. 2011;22:190–193.
4. Rosenfeld PJ, Shapiro H, Tuomi L, Webster M, Elledge J, Blodi B. Characteristics of patients losing vision after 2 years of monthly dosing in the phase III ranibizumab clinical trials. *Ophthalmology*. 2011;118:523–530.
5. Day S, Acquah K, Lee PP, Mruthyunjaya P, Sloan FA. Medicare costs for neovascular age-related macular degeneration, 1994-2007. *Am J Ophthalmol*. 2011;152:1014–1020.
6. Joachim N, Mitchell P, Burlutsky G, Kifley A, Wang JJ. The incidence and progression of age-related macular degeneration over 15 years: the Blue Mountains Eye Study. *Ophthalmology*. 2015;122:2482–2489.
7. Hogan MJ. Role of the retinal pigment epithelium in macular disease. *Trans Am Acad Ophthalmol Otolaryngol*. 1972;76:64–80.
8. Curcio CA, Johnson M, Huang J-D, Rudolf M. Aging, age-related macular degeneration, and the response-to-retention of apolipoprotein B-containing lipoproteins. *Prog Ret Eye Res*. 2009;28:393–422.
9. Johnson LV, Forest DL, Banna CD, et al. Cell culture model that mimics drusen formation and triggers complement activation associated with age-related macular degeneration. *Proc Natl Acad Sci U S A*. 2011;108:18277–18282.
10. Crabb JW, Miyagi M, Gu X, et al. Drusen proteome analysis: an approach to the etiology of age-related macular degeneration. *Proc Natl Acad Sci U S A*. 2002;99:14682–14687.
11. Tabas I, Williams KJ, Boren J. Subendothelial lipoprotein retention as the initiating process in atherosclerosis: update and therapeutic implications. *Circulation*. 2007;116:1832–1844.
12. Nan R, Tetchner S, Rodriguez E, et al. Zinc-induced self-association of complement C3b and Factor H: implications for inflammation and age-related macular degeneration. *J Biol Chem*. 2013;288:19197–19210.
13. Lengyel I, Flinn JM, Peto T, et al. High concentration of zinc in sub-retinal pigment epithelial deposits *Exp Eye Res*. 2007;84:772–780.
14. Flinn JM, Kakalec P, Tappero R, Jones B, Lengyel I. Correlations in distribution and concentration of calcium, copper and iron with zinc in isolated extracellular deposits associated with age-related macular degeneration. *Metallomics Integrat Biometal Sci*. 2014;6:1223–1228.
15. Thompson RB, Reffatto V, Bundy JG, et al. Identification of hydroxyapatite spherules provides new insight into subretinal pigment epithelial deposit formation in the aging eye. *Proc Natl Acad Sci U S A*. 2015;112:1565–1570.
16. Amin S, Chong NH, Bailey TA, et al. Modulation of sub-RPE deposits in vitro: a potential model for age-related macular degeneration. *Invest Ophthalmol Vis Sci*. 2004;45:1281–1288.
17. Fernandez-Godino R, Garland DL, Pierce EA. A local complement response by RPE causes early-stage macular degeneration. *Hum Mol Genet*. 2015;24:5555–5569.
18. Pauleikhoff D, Zuels S, Sheraidah GS, Marshall J, Wessing A, Bird AC. Correlation between biochemical composition and fluorescein binding of deposits in Bruch's membrane. *Ophthalmology*. 1992;99:1548–1553.
19. Curcio CA, Millican CL, Bailey T, Kruth HS. Accumulation of cholesterol with age in human Bruch's membrane. *Invest Ophthalmol Vis Sci*. 2001;42:265–274.
20. Mullins RF, Russell SR, Anderson DH, Hageman GS. Drusen associated with aging and age-related macular degeneration contain proteins common to extracellular deposits associated with atherosclerosis, elastosis, amyloidosis, and dense deposit disease. *FASEB J*. 2000;14:835–846.
21. Mamballikalathil I, Mann C, Guidry C. Tractional force generation by porcine Müller cells: stimulation by retinal pigment epithelial cell-secreted growth factor. *Invest Ophthalmol Vis Sci*. 2000;41:529–536.
22. Maminishkis A, Chen S, Jalickee S, et al. Confluent monolayers of cultured human fetal retinal pigment epithelium exhibit morphology and physiology of native tissue. *Invest Ophthalmol Vis Sci*. 2006;47:3612–3624.
23. Fuchs U, Kivelä T, Tarkkanen A. Cytoskeleton in normal and reactive human retinal pigment epithelial cells. *Invest Ophthalmol Vis Sci*. 1991;32:3178–3186.
24. Peng S, Rao VS, Adelman RA, Rizzolo LJ. Claudin-19 and the barrier properties of the human retinal pigment epithelium. *Invest Ophthalmol Vis Sci*. 2011;52:1392–1403.
25. Hu J, Bok D. A cell culture medium that supports the differentiation of human retinal pigment epithelium into functionally polarized monolayers. *Mol Vis*. 2001;7:14–19.
26. Nawrot M, West K, Huang J, et al. Cellular retinaldehyde-binding protein interacts with ERM-binding phosphoprotein 50 in retinal pigment epithelium. *Invest Ophthalmol Vis Sci*. 2004;45:393–401.
27. Li CM, Presley JB, Zhang X, et al. Retina expresses microsomal triglyceride transfer protein: implications for age-related maculopathy. *J Lipid Res*. 2005;46:628–640.
28. Lanzirotti A, Newville M, Manoukian L, Lange K. High-speed, coupled micro-beam XRD/XRF/XAFS mapping at GSECARS: APS beamline 13-ID-E. *Clay and Clay Minerals*. 2016;21:53–64.
29. Curcio CA, Messinger JD, Sloan KR, McGwin G Jr, Medeiros NE, Spaide RF. Subretinal drusenoid deposits in non-neovascular age-related macular degeneration: morphology, prevalence, topography, and biogenesis model. *Retina*. 2013;33:265–276.
30. Zanzottera EC, Messinger JD, Ach T, Smith RT, Freund KB, Curcio CA. The Project MACULA retinal pigment epithelium grading system for histology and optical coherence tomography in age-related macular degeneration. *Invest Ophthalmol Vis Sci*. 2015;56:3253–3268.
31. Vogt SD, Curcio CA, Wang L, et al. Retinal pigment epithelial expression of complement regulator CD46 is altered early in the course of geographic atrophy. *Exp Eye Res*. 2011;93:413–423.
32. Malek G, Li C-M, Guidry C, Medeiros NE, Curcio CA. Apolipoprotein B in cholesterol-containing drusen and basal deposits in eyes with age-related maculopathy. *Am J Pathol*. 2003;162:413–425.
33. Oak ASW, Messinger JD, Curcio CA. Subretinal drusenoid deposits: further characterization by lipid histochemistry. *Retina*. 2014;34:825–826.
34. Moore DJ, Hussain AA, Marshall J. Age-related variation in the hydraulic conductivity of Bruch's membrane. *Invest Ophthalmol Vis Sci*. 1995;36:1290–1297.
35. Newsome DA, Huh W, Green WR. Bruch's membrane age-related changes vary by region. *Curr Eye Res*. 1987;6:1211–1221.
36. Ramrattan RS, van der Schaft TL, Mooy CM, de Bruijn WC, Mulder PGH, de Jong PTVM. Morphometric analysis of Bruch's membrane, the choriocapillaris, and the choroid in aging. *Invest Ophthalmol Vis Sci*. 1994;35:2857–2864.
37. Curcio CA, Johnson M, Rudolf M, Huang J-D. The oil spill in ageing Bruch's membrane. *Br J Ophthalmol*. 2011;95:1638–1645.
38. Bergen AA, Plomp AS, Schuurman EJ, et al. Mutations in ABCC6 cause pseudoxanthoma elasticum. *Nature Genet*. 2000;25:228–231.

Investigative Ophthalmology & Visual Science

39. Mullins RF, Johnson MN, Faidley EA, Skeie JM, Huang J. Choriocapillaris vascular dropout related to density of drusen in human eyes with early age-related macular degeneration. *Invest Ophthalmol Vis Sci*. 2011;52:1606–1612.
40. Chirco KR, Tucker BA, Stone EM, Mullins RF. Selective accumulation of the complement membrane attack complex in aging choriocapillaris. *Exp Eye Res*. 2015.
41. Whitmore SS, Sohn EH, Chirco KR, et al. Complement activation and choriocapillaris loss in early AMD: implications for pathophysiology and therapy. *Prog Retin Eye Res*. 2015; 45:1–29.
42. Curcio CA, Presley JB, Millican CL, Medeiros NE. Basal deposits and drusen in eyes with age-related maculopathy: evidence for solid lipid particles. *Exp Eye Res*. 2005;80:761–775.
43. Sarks JP, Sarks SH, Killingsworth MC. Evolution of geographic atrophy of the retinal pigment epithelium. *Eye*. 1988;2:552–577.
44. Sarks S, Cherepanoff S, Killingsworth M, Sarks J. Relationship of basal laminar deposit and membranous debris to the clinical presentation of early age-related macular degeneration. *Invest Ophthalmol Vis Sci*. 2007;48:968–977.
45. Zweifel SA, Imamura Y, Spaide TC, Fujiwara T, Spaide RF. Prevalence and significance of subretinal drusenoid deposits (reticular pseudodrusen) in age-related macular degeneration. *Ophthalmology*. 2010;117:1775–1781.
46. Greferath U, Guymer RH, Vessey KA, Brassington K, Fletcher EL. Correlation of histologic features with in vivo imaging of reticular pseudodrusen. *Ophthalmology*. 2016;123:1320–1331.
47. Boskey AL, Posner AS. Conversion of amorphous calcium phosphate to microcrystalline hydroxyapatite. A pH-dependent, solution-mediated, solid-solid conversion. *J Physical Chem*. 1973;77:2313–2317.
48. Goldberg M, Boskey AL. Lipids and biomineralizations. *Prog Histochem Cytochem*. 1996;31:1–187.
49. Colfen H. Biomineralization: a crystal-clear view. *Nature Mater*. 2010;9:960–961.
50. Farkas TG, Sylvester V, Archer D. The ultrastructure of drusen. *Am J Ophthalmol*. 1971;71:1196–1205.
51. Ethier CR, Johnson M, Ruberti J. Ocular biomechanics and biotransport. *Annu Rev Biomed Engineer*. 2004;6:249–273.
52. Pikuleva I, Curcio CA. Cholesterol in the retina: the best is yet to come. *Prog Ret Eye Res*. 2014;41:64–89.
53. Schlanitz FG, Baumann B, Kundi M, et al. Drusen volume development over time and its relevance to the course of age-related macular degeneration [published online ahead of print April 4, 2016]. *Br J Ophthalmol*. doi:10.1136/bjophthalmol-2016-308422.
54. Balaratnasingam C, Yannuzzi LA, Curcio CA, et al. Associations between retinal pigment epithelium and drusen volume changes during the lifecycle of large drusenoid pigment epithelial detachments. *Invest Ophthalmol Vis Sci*. 2016;57: 5479–5489.
55. Mukherjee S, King JL, Guidry C. Phenotype-associated changes in retinal pigment epithelial cell expression of insulin-like growth factor binding proteins. *Invest Ophthalmol Vis Sci*. 2009;50:5449–5455.
56. Nazari H, Zhang L, Zhu D, et al. Stem cell based therapies for age-related macular degeneration: the promises and the challenges. *Prog Retin Eye Res*. 2015;48:1–39.
57. Neale BM, Fagerness J, Reynolds R, et al. Genome-wide association study of advanced age-related macular degeneration identifies a role of the hepatic lipase gene (LIPC). *Proc Natl Acad Sci U S A*. 2010;107:7395–7400.
58. Chen W, Stambolian D, Edwards AO, et al. Genetic variants near TIMP3 and high-density lipoprotein-associated loci influence susceptibility to age-related macular degeneration. *Proc Natl Acad Sci U S A*. 2010;107:7401–7406.
59. Guyard-Dangremont V, Desrumaux C, Gambert P, Lallemant C, Lagrost L. Phospholipid and cholesteryl ester transfer activities in plasma from 14 vertebrate species. Relation to atherogenesis susceptibility. *Comp Biochem Physiol B*. 1998; 120:517–525.
60. Spaide RF, Armstrong D, Browne R. Continuing medical education review: choroidal neovascularization in age-related macular degeneration—what is the cause? *Retina*. 2003;23: 595–614.
61. Schaal KB, Rosenfeld PJ, Gregori G, Yehoshua Z, Feuer WJ. Anatomic clinical trial endpoints for nonexudative age-related macular degeneration. *Ophthalmology*. 2016;123:1060–1079.
62. Vavvas DG, Daniels AB, Kapsala ZG, et al. Regression of some high-risk features of age-related macular degeneration (AMD) in patients receiving intensive statin treatment. *EBioMedicine*. 2016;5:198–203.

Investigative Ophthalmology & Visual Science